Charge-transfer processes in $F^{2+}+H \rightarrow F^{+}+H^{+}$ collisions and the reverse process at low-keV energies

C. M. Dutta,[1] J. P. Gu,[2] G. Hirsch,[2,*] R. J. Buenker,[2] P. Nordlander,[1] and M. Kimura[3]
[1]*Department of Physics and Astronomy, Rice University, M.S. 61, Houston, Texas 77251-1892, USA*
[2]*Fachbereich C-Mathematik and Naturwissenshaften, Bergische Universitaet Wuppertal, D-42097 Wuppertal, Germany*
[3]*Graduate School of Sciences, Kyushu University, Hakozaki Fukuoka 812-8581, Japan*
(Received 19 July 2005; published 21 November 2005)

Theoretical investigations on single charge-transfer processes in collisions of $F^{2+}+H \rightarrow F^{+}+H^{+}$ and its reverse process have been carried out at collision energies from 20 eV/u to 10 keV/u. The molecular orbital expansion method within the semiclassical impact parameter formalism has been employed for the scattering dynamics, while the *ab initio* multireference single- and double-excitation configuration interaction (MRD-CI) method was adopted for determination of molecular electronic states. The initial channels correspond to the quintet and triplet states for the corresponding collision processes, respectively. Four molecular states in the quintet manifold and eight molecular states in the triplet manifold were coupled. In the quintet manifold, the charge-transfer cross sections for $F^{2+}+H \rightarrow F^{+}+H^{+}$ range from 1.3×10^{-22} cm^2 at 20 eV/u to 2.5×10^{-15} cm^2 at 10 keV/u. The cross sections of the reverse process, $F^{+}+H^{+} \rightarrow F^{2+}+H$, range from 3.0×10^{-22} cm^2 to 2.3×10^{-15} cm^2 in the same energy range. In the triplet states, the charge-transfer cross sections for $F^{2+}+H \rightarrow F^{+}+H^{+}$ range from 1.1×10^{-18} cm^2 to 2.5×10^{-16} cm^2, and its reverse process gives charge-transfer cross sections ranging from 1.7×10^{-24} cm^2 to 1.5×10^{-17} cm^2.

DOI: 10.1103/PhysRevA.72.052715 PACS number(s): 34.10.+x, 34.50.Fa, 34.70.+e

I. INTRODUCTION

Research on charge-transfer processes has been a central topic in atomic collision dynamics over the past decades. The topic is of fundamental importance for understanding basic atomic physics and also of crucial importance in various applications. Although experimental and theoretical data for charge-transfer cross sections for heavy ion collisions are important in many fields, the investigation for heavy ions, that is, ions heavier than carbon and oxygen, have been relatively scarce. A particularly interesting example in this category is fluorine.

Fluorine atoms have previously been thought to be rare in the astrophysical environment, but recently found to be abundant in giant stars [1]. Collision and charge-transfer processes involving fluorine atoms may play an important role for ionic spatial and energy distributions of such objects. Fluorine atoms and ions are also notorious for their negative environmental impact, such as the ozone depletion in the stratosphere [2], which provides yet another motivation for studying their dynamics and reactivity in collisions with other atoms. Per-fluorocarbons (PFCs) are known to be one of the most efficient etching gases [3] for semiconductor industries, and hence, electron and ion collisions with PFCs and their derivatives are of particular importance for evaluation of low-temperature plasma behavior. In addition, fluorine atoms and ions play an important role in biology and living cells [4]. These examples clearly illustrate the importance of studying charge-transfer reactions in collisions involving fluorine atoms [5–9]. To the best of our knowledge, there are no experimental data available for this collision. The present theoretical calculation of charge-transfer cross section attempts to supply the needed data and stimulate experimental studies.

We have earlier reported an investigation of the single charge-transfer processes in collisions of F^{2+} ions with a helium atom and its reverse process [9], providing comprehensive theoretical cross section data. In this paper, we present a study on single charge-transfer processes in collisions between F^{2+} ions and a hydrogen atom and its reverse process, and provide detailed cross section data. The FH^{2+} molecule exists in low-lying singlet, triplet and quintet states. Since our interest is primarily concerned with charge-transfer within the same spin-manifold, we do not include spin-orbit coupling in the collision treatment. As will be seen below, the lowest energy singlet configurations that separate to FH^{2+} and H at large nuclear separation lies about 4.2 eV above the lowest energy of the corresponding triplet and quintet configurations. Therefore, we do not include the singlet manifold in the collision treatment, and focus on collisions involving the triplet and quintet states at collision energies from 20 eV/u to 10 keV/u. In Sec. II, we briefly explain how the molecular orbitals and the energies of the corresponding molecular states are obtained, and in Sec. III we present detailed cross sections for the charge-transfer processes. Finally, in Sec. IV, we provide our conclusions and also some thought on how to compare the calculated cross sections with measurements.

II. THEORY

We use the molecular-orbital close-coupling (MOCC) method, together with the semi-classical impact parameter approximation in which the nuclear trajectory is assumed to be a straight line. We chose this approach because of the

*Deceased.

TABLE I. MO states, asymptotic configurations, and calculated and measured relative energies. The measured energies are obtained from [42]. The energies of different J multiplicity were averaged.

MO	Asymptotic configuration	Measured energy (cm^{-1})	Calculated energy (cm^{-1})
$1\,^3\Sigma^-, 1\,^3\Pi$	$F^+(2s^2 2p^4)+H^+$	0	46
$1\,^1\Sigma^+, 1\,^1\Pi, 1\,^1\Delta$	$F^+(2s^2 2p^4)+H^+$	20873	21204
$2\,^1\Sigma^+$	$F^+(2s^2 2p^4)+H^+$	44919	45263
$1\,^3\Sigma^+, 2\,^3\Pi$	$F^+(2s^1 2p^5)+H^+$	164798	164331
$2\,^3\Sigma^-, 1\,^5\Sigma^-$	$F^{2+}(2s^2 2p^3)+H$	172511	169724
$2\,^5\Sigma^-$	$F^+(2s^2 2p^3 3s^1)+H^+$	176654	174146
$3\,^3\Sigma^-$	$F^+(2s^2 2p^3 3s^1)+H^+$	182865	180615
$3\,^5\Sigma^-, 1\,^5\Pi$	$F^+(2s^2 2p^3 3p^1)+H^+$	202610	200813
$1\,^1\Sigma^-, 2\,^1\Pi$	$F^{2+}(2s^2 2p^3)+H$	206595	204692
$2\,^1\Delta, 4\,^3\Sigma^-$		206595	204692
$3\,^3\Pi, 1\,^3\Delta$		206595	204692

following reasons. In the intermediate collision energy region of low keV, the use of the molecular orbital basis set is appropriate, since at collision velocity v less than v_{el}, the colliding particles spend enough time in the vicinity of each other to form a quasimolecule. Also the validity of the straight line trajectory for calculation of total cross section has been established [10–15] even at low eV energies. The method we use has been applied to calculation of charge transfer cross sections in numerous cases of ion-atom/molecule collisions (for some examples, see [16–29]). Some of these examples include charge asymmetric cases such as silicon and its ion colliding with He [27,28] and oxygen ions with H_2 [26] and the results were usually in good agreement with available experiments. If a basis set is complete, any of them should lead to similar results [30]. The choice of basis set depends on how to describe the collision processes by a relatively small number of basis functions. We chose the molecular orbital basis set in the present work. At higher collision energies, excitation and ionization become more important than charge transfer, and the number of molecular orbitals to be coupled become large. Therefore, alternative approaches such as using Sturmian basis sets [31–33] or Monte Carlo method are often used [34,35].

Molecular states: The FH^{2+} molecular wave functions and their adiabatic potentials were generated by employing the *ab initio* multireference single- and double-excitation configuration interaction (MRD-CI) method [36–38] with the configuration selection at a threshold of $5.0\times10^{-8}E_h$, and energy extrapolation, using the Table CI algorithm. The basis set was obtained from the Extensible Computational Chemistry Environment Basis Set Database, Version 1.0, as developed and distributed by the Molecular Science Computing Facility, and Environmental and Molecular Sciences Laboratory. This approach gives results for the energies and couplings which are very close to the results for full CI [39–41]. The same basis set was used for F in our earlier work [9].

Table I shows the molecular states, and their asymptotic systems at large internuclear separation, R. Also in this table the relative energy levels were compared with observed energy levels [42]. From this table, we see that the FH^{2+} molecule exists in a number of low-lying singlet, triplet and quintet states.

Scattering dynamics: We used the semiclassical molecular-orbital close-coupling (MOCC) method, together with the straight-line trajectory, for investigating scattering dynamics of the collision [43]. The total scattering wave functions were expanded in terms of products of time dependent expansion coefficients (probability amplitudes), electronic states and the plane wave type electron translation factors (ETF's), where ETF's were expanded with respect to velocity and included up to the first order of the velocity. The total wave function was substituted into the time-dependent Schrödinger equation, thus yielding the first-order coupled equations. The coupled equations were solved numerically to obtain the probability amplitude and then following the usual procedure, we determine cross sections for charge-transfer. Since we do not include the spin-orbit coupling in our Hamiltonian, we consider the charge-transfer processes within each spin manifold separately. We do not include the singlet manifolds in the present study, since the singlet ground state that separates to F^{2+} and H lies above the molecular energy levels considered here.

III. RESULTS AND DISCUSSION

In the following two subsections we present the results of our calculations for the charge-transfer cross sections within the quintet and triplet manifolds respectively.

A. Quintet states

We coupled four quintet states in Table I, namely, $1\,^5\Sigma^-$, $2\,^5\Sigma^-$, $3\,^5\Sigma^-$, and $1\,^5\Pi$ states. The $3\,^5\Sigma^-$ and $1\,^5\Pi$ states are degenerate at large internuclear separation, R, separating to $F^+(2s^2 2p^3 3p)$ and H^+ ions. Figure 1 shows the molecular potentials of these states. We observe no apparent avoided crossings among those states. The $1\,^5\Sigma^-$ state has a very shallow well of depth $\sim$0.43 eV around $R=4.5$ a.u. The radial and rotational coupling matrix elements among these four states are shown in Figs. 2 and 3, respectively.

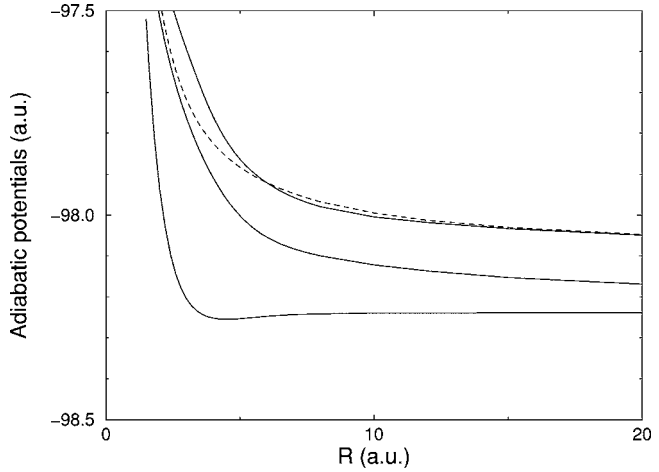

FIG. 1. The relative energy levels of the FH^{2+} molecule in the quintet manifold. The solid lines are from the bottom $1\,^5\Sigma^-$, $2\,^5\Sigma^-$, and $3\,^5\Sigma^-$, respectively, and the dotted line is $1\,^5\Pi$.

First, we consider

$$F^{2+} + H \rightarrow F^{+} + H^{+}. \tag{1}$$

In this case, the entrance channel is $1\,^5\Sigma^-$, and all other outgoing channels correspond to those of charge-transfer, producing F^+ and H^+ ions. Figure 4 shows calculated single charge-transfer cross sections, together with partial cross sections. Charge transfer to the nearest state, $2\,^5\Sigma^-$, dominates in the entire energy range considered here, but transfer to other states increases with energy. The total cross section increases rapidly from 1.4×10^{-22} cm^2 at 20 eV/u to 2.5×10^{-15} cm^2 at 10 keV/u.

Next, we consider the reverse process, namely,

$$F^{+} + H^{+} \rightarrow F^{2+} + H. \tag{2}$$

The incoming channel is the $2\,^5\Sigma^-$ state in this case, and the charge-transfer state is the $1\,^5\Sigma^-$ state. The remaining two states correspond to excitation of F^+ ions.

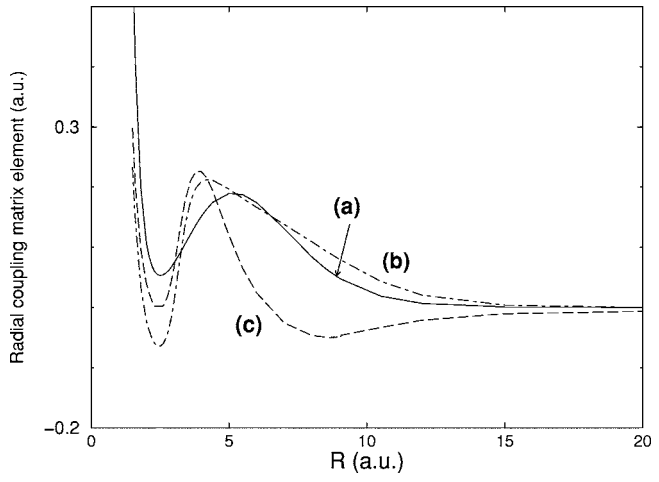

FIG. 2. Radial coupling matrix elements in the quintet manifold. (a) $1\,^5\Sigma^- - 2\,^5\Sigma^-$, (b) $1\,^5\Sigma^- - 3\,^5\Sigma^-$, and (c) $1\,^5\Sigma^- - 4\,^5\Sigma^-$.

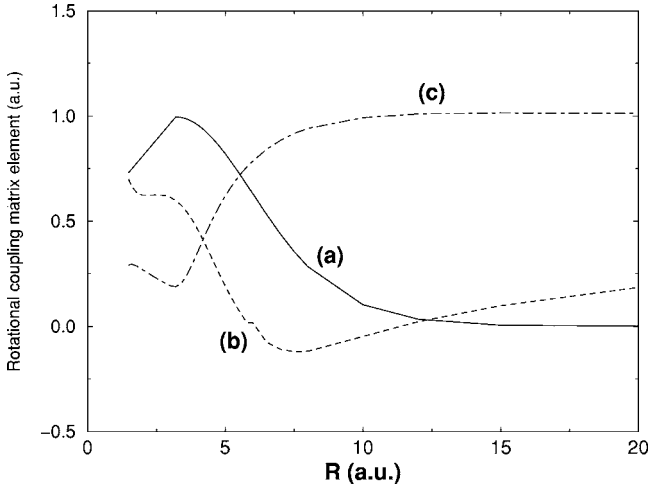

FIG. 3. Rotational coupling matrix elements in the quintet manifold. (a) $1\,^5\Sigma^- - 1\,^5\Pi$, (b) $2\,^5\Sigma^- - 1\,^5\Pi$, and (c) $3\,^5\Sigma^- - 1\,^5\Pi$, respectively.

Figure 5 shows the charge-transfer cross sections and the excitation cross sections. The charge-transfer cross sections are small at low energies (3.0×10^{-22} cm^2 at 20 eV/u) by several orders of magnitude, compared to the excitation cross sections (2.3×10^{-15} cm^2 at the same energy), but increase rapidly with energy. The charge-transfer cross sections remain nearly constant beyond ~5 keV/u, while the excitation cross sections saturate at a much lower kinetic energy around ~0.8 keV/u. This may be understood from the radial coupling matrix elements shown in Fig. 2. Radial couplings are more effective in charge-transfer than rotational coupling at low collision energies. In Fig. 2, the radial coupling matrix elements between the incoming $2\,^5\Sigma^-$ state and the excited F^+ states [curves (b) and (c)] are longer-range couplings than that between the the incoming and charge-transfer $1\,^5\Sigma^-$ state [curve (a)]. Therefore, at low collision energies the excitation cross sections become relatively larger than those for charge

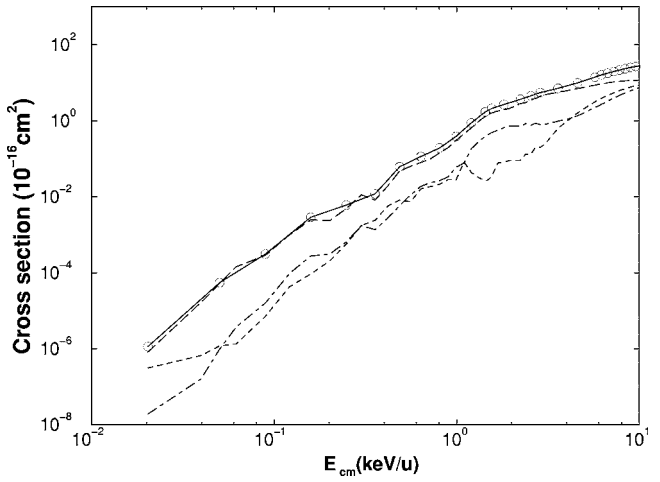

FIG. 4. $F^{2+}+H$ collision in the quintet manifold. The partial cross sections are long dash for $2\,^5\Sigma^-$, chain for $1\,^5\Pi$, and dotted line for $3\,^5\Sigma^-$, respectively. The total transfer cross sections, shown with a solid line with circles, are the sum of these partial cross sections.

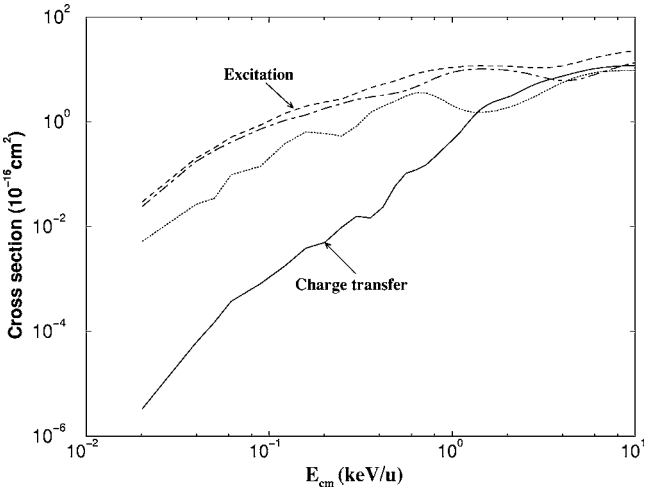

FIG. 5. $F^+ + H^+$ collision in the quintet manifold. The partial cross sections are a full line for $1\ ^5\Sigma^-$, dotted line for $3\ ^5\Sigma^-$, and chain for $1\ ^5\Pi$. The total charge-transfer cross sections: full line; the excitation cross sections: dashed line.

transfer. The magnitudes of the radial couplings, curves (a) and (b) are comparable in the $R<10$ a.u. range and therefore, as the collision energy increases, excitation and charge-transfer cross sections both behave in similar manner.

B. Triplet states

Figure 6(a) shows the adiabatic potentials of four $^3\Sigma^-$ states and one $^3\Sigma^+$ state, while Fig. 6(b) shows three $^3\Pi$ states. The $^3\Sigma^+$ state does not directly couple with $^3\Sigma^-$ states, but it can couple via the $^3\Pi$ states. Since the $1\ ^3\Sigma^+$ state is degenerate with $2\ ^3\Pi$ at large R, and is energetically close to the entrance channel of F^{2+}/H, we included the $1\ ^3\Sigma^+$ state shown by a dotted line in Fig. 6(a). We did not include $1\ ^3\Delta$, since it does not directly couple with the incoming channels,

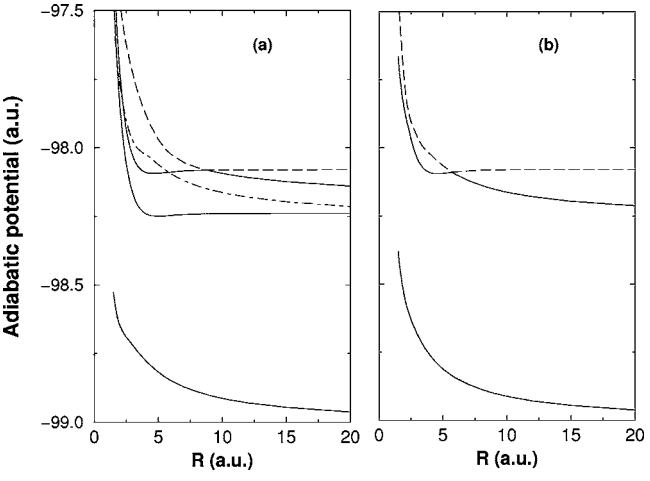

FIG. 6. (a) Adiabatic potentials of the $^3\Sigma$ states. Full lines from the bottom correspond to $1\ ^3\Sigma^-$, $2\ ^3\Sigma^-$, and $3\ ^3\Sigma^-$. The dot-dashed line is for $1\ ^3\Sigma^+$, and the long dashed line represents $4\ ^3\Sigma^-$. (b) Adiabatic potentials of the $^3\Pi$ states. The full lines are from the bottom $1\ ^3\Pi$, and $2\ ^3\Pi$. The long dashed line is $3\ ^3\Pi$.

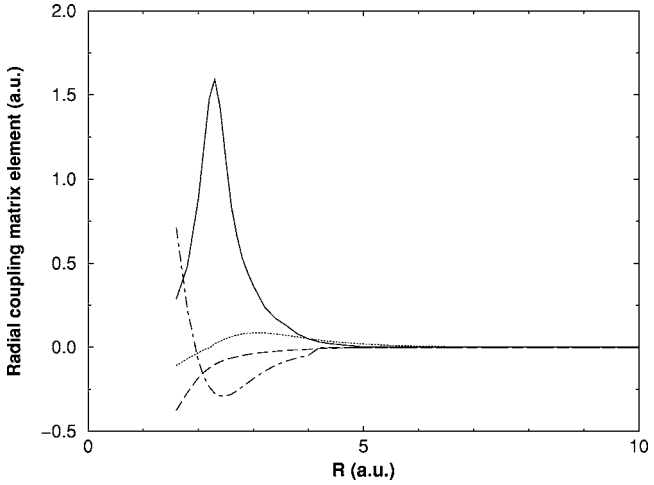

FIG. 7. Radial coupling matrix elements in the triplet manifold: full line, $2\ ^3\Pi - 3\ ^3\Pi$; dotted line, $1\ ^3\Sigma^- - 2\ ^3\Sigma^-$; dash line, $3\ ^3\Sigma^- - 4\ ^3\Sigma^-$; chain, $2\ ^3\Sigma^- - 4\ ^3\Sigma^-$.

and also the energy level is not close to the incoming channels we consider here. The $3\ ^3\Sigma^-$ state and the $4\ ^3\Sigma^-$ state have an avoided crossing (the energy gap of 7×10^{-5} a.u. at $R=8.8$ a.u.). In Fig. 6(b), the $3\ ^3\Pi$ state has an avoided crossing (the energy gap of 8×10^{-3} a.u. at $R=5.5$ a.u.) with $2\ ^3\Pi$ state. Therefore, we constructed pseudo–$3\ ^3\Sigma^-$ and pseudo–$4\ ^3\Sigma^-$ states, and also pseudo–$2\ ^3\Pi$ and pseudo–$3\ ^3\Pi$ states by exchanging the potential curves as well as the coupling matrix elements involving these states when $R \leqslant R_x$, where R_x is the position of each avoided crossing. This is to ensure that the transition at R_x is 100% between the states. Among the eight states we coupled, the $2\ ^3\Sigma^-$, $4\ ^3\Sigma^-$, and the $3\ ^3\Pi$ states separate to F^{2+} and H at large R, and the other channels all separate to F^+ and H^+ ions. The $1\ ^3\Sigma^-$ and $1\ ^3\Pi$ states are degenerate at large R. Figure 7 shows some representatives of the radial coupling matrix elements, while some of the rotational coupling matrix elements are shown in Fig. 8. The rotational coupling matrix elements between $1\ ^3\Sigma^-$ and $1\ ^3\Pi$, and also between $1\ ^3\Sigma^+$ and $2\ ^3\Pi$ are large and nearly constant at large R, because of their degeneracy. The other rotational coupling matrix elements are relatively small and become negligible beyond $R\sim12$ a.u.

First, we consider

$$F^{2+} + H \rightarrow F^+ + H^+. \tag{3}$$

The entrance channel is the $2\ ^3\Sigma^-$ state, and $1\ ^3\Sigma^-$, $3\ ^3\Sigma^-$, $1\ ^3\Sigma^+$, $1\ ^3\Pi$ and $2\ ^3\Pi$ states correspond to single charge-transfer states. The $4\ ^3\Sigma^-$ and $3\ ^3\Pi$ channel lead to production of excited F^{2+} ions and the ground state H atoms. Figure 9 shows the partial cross sections for each outgoing channel. The dominant charge-transfer channels are the $1\ ^3\Sigma^+$ and $2\ ^3\Pi$ states. These two states are degenerate at large R, and are energetically close to the incoming channel. All partial cross sections except those for $3\ ^3\Sigma^-$ show a similar behavior, that is, a sharp rise up to 1 keV/u followed by a level-off remaining almost constant, while the cross section for the $3\ ^3\Sigma^-$ state shows a sharp increase up to 0.5 keV/u, and after that, a gradual decrease before again increasing. The cross

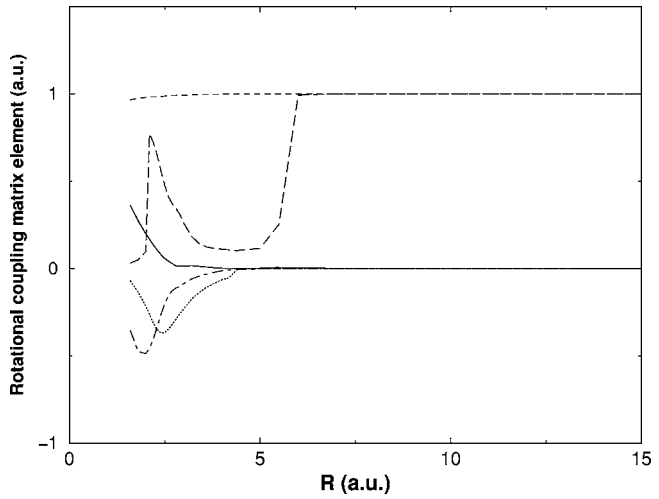

FIG. 8. Rotational coupling matrix elements in the triplet manifold. Solid line, $3\,^3\Sigma^- - 2\,^3\Pi$; dotted line, $2\,^3\Sigma^- - 3\,^3\Pi$, chain, $2\,^3\Sigma^+ - 2\,^3\Pi$; long dashed line, $2\,^3\Sigma^- - 1\,^3\Sigma^+$; and the upper dashed line, $1\,^3\Sigma^- 1\,^3\Pi$ that are degenerated.

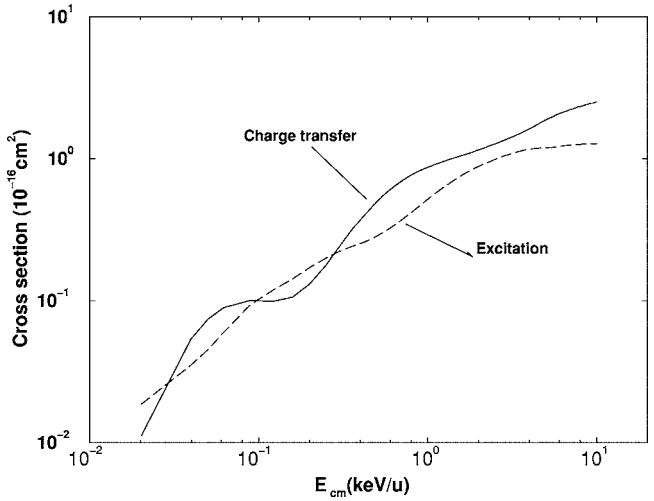

FIG. 10. Charge transfer and excitation cross sections for $F^{2+}+H \rightarrow F^{+}+H^{+}$ in the triplet manifold. Solid line with circles, charge-transfer, and solid line, excitation, respectively.

sections for the $1\,^3\Pi$ and $1\,^3\Sigma^-$ show strong interference patterns around 1.5 keV/u caused by relatively effective couplings between them.

Figure 10 shows the total charge-transfer and excitation cross sections. At low energies, the excitation and charge-transfer cross sections are comparable, but the charge-transfer cross sections rapidly increase, and are found to become larger than the excitation cross sections beyond ~0.5 keV/u.

Next, we consider the reverse case, i.e.,

$$F^+ + H^+ \rightarrow F^{2+} + H. \tag{4}$$

In this case, the incoming channel is either $1\,^3\Sigma^-$ or $1\,^3\Pi$. We studied each case separately, and the results of charge-transfer and excitation cross sections are compared in Fig. 11. We observe that the cross sections for each incoming channel did not differ greatly, and show similar magnitudes and energy-dependence. We took the average of the cross sections calculated for the $1\,^3\Sigma^-$ and $1\,^3\Pi$ incoming channels, and the resulting charge-transfer cross sections are shown in Fig. 12. The resulted charge-transfer cross sections range from 1.7×10^{-24} cm^2 at 20 eV/u and 1.5×10^{-17} cm^2 at 10 keV, while the excitation cross sections are slightly smaller at the beginning with a value of 3.7×10^{-25} cm^2 at 20 eV/u, but rapidly increase and reach 2.4×10^{-17} cm^2 at 10 keV.

We calculated charge transfer cross sections separately for each multiplet. However, measuring cross sections experimentally for each multiplet is difficult. One would expect to be dealing with low ion fluxes, that would make high resolution spectroscopic interrogation of the state of F^{2+} very difficult. Likewise, the concentration and perhaps the short

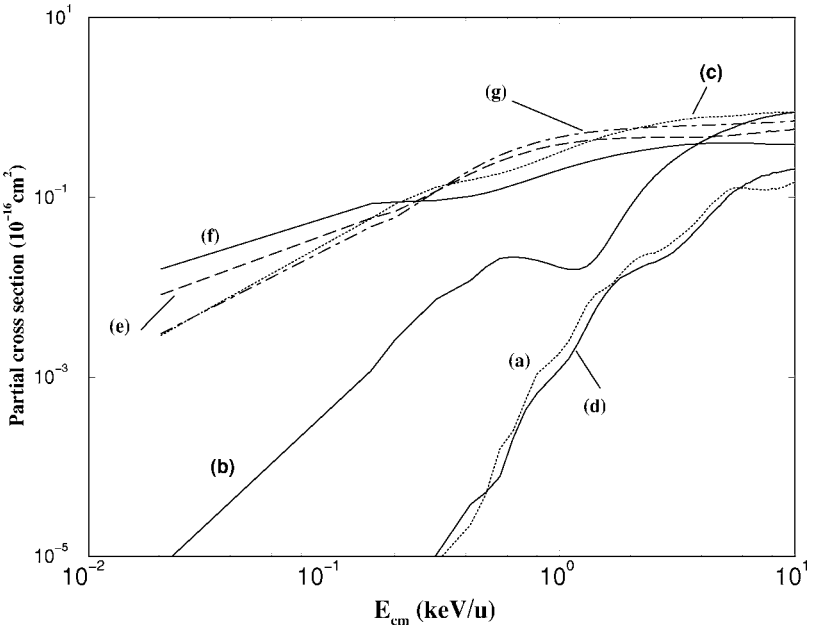

FIG. 9. Partial cross sections for each outgoing channel in $F^{2+}+H \rightarrow F^{+}+H^{+}$ in the triplet manifold. (a) $1\,^3\Sigma^-$, (b) $3\,^3\Sigma^-$, (c) $4\,^3\Sigma^-$, (d) $1\,^3\Pi$, (e) $2\,^3\Pi$, (f) $3\,^3\Pi^-$, and (g) $1\,^3\Sigma^+$, respectively.

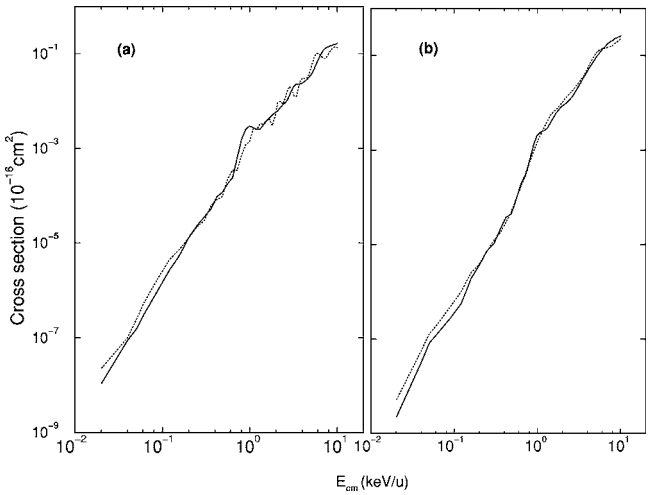

FIG. 11. Charge transfer (solid line) and excitation (dotted line) cross sections in $F^+ + H^+ \rightarrow F^{2+} + H$ (a) for the incoming channel of $1\,^3\Sigma^-$, and (b) for $1\,^3\Pi$, respectively.

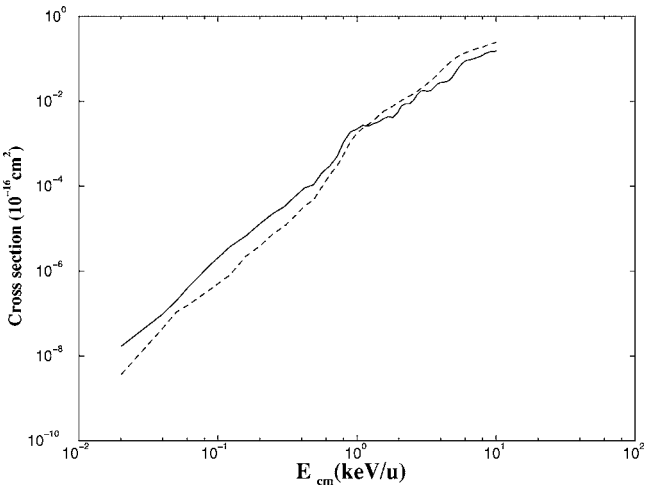

FIG. 12. $F^+ + H^+ \rightarrow F^{2+} + H$ in the triplet manifold. Charge transfer cross sections (solid line), and excitation cross sections (dotted line). The cross sections are the averaged ones for the incoming channel of $1\,^3\Sigma^-$ and $1\,^3\Pi$ shown in Fig. 11.

lifetime of the quasimolecule would make its spectroscopy very difficult. Also, the experiment has to be at very low energies. For neutrals you could look at the deflection of the reagents in a magnetic field to distinguish different multiplets. The effect of the charge complicates the deflection due to the spin, but with very high energy resolution one might be able to see effects due to different spin configurations. However, the required resolution is probably very high and obtaining this resolution could be difficult. Alternately, it might be possible to use the calculated potential curves. Since the molecular potential curves for HF^{2+} are known, one could measure the kinetic energies of the F^+ and H^+ after the collision and it may be possible to correlate the kinetic energies with the potential curves. However, this sort of approach would only be usable for very low energy collisions, since the energy differences among the potentials of different multiplets are less than a few eV.

IV. CONCLUSION

We calculated single charge-transfer and excitation cross sections in collisions of $F^{2+} + H \rightarrow F^+ + H$ and the reverse collisions at collision energies of 20 eV/u to 10 keV/u, in the quintet and triplet states. In the quintet state collisions, the charge-transfer cross sections in $F^{2+} + H \rightarrow F^+ + H$ are 1.3×10^{-22} cm^2 at 20 eV and rapidly increase to 2.5×10^{-15} cm^2 at 10 keV. In the reverse process, the charge-transfer cross sections range from 3.0×10^{-22} cm^2 to 2.3×10^{-15} cm^2. In the triplet state, the charge-transfer cross sections for $F^{2+} + H \rightarrow F^+ + H^+$ collisions range from 1.1×10^{-18} cm^2 at 20 eV/u and 2.5×10^{-16} cm^2 at 10 keV, and its reverse process yields the charge-transfer cross sections ranging from 1.7×10^{-24} cm^2 to 1.5×10^{-17} cm^2. The excitation cross sections range from 3.7×10^{-25} cm^2 at 20 eV/u to 2.4×10^{-17} cm^2 at 10 keV.

ACKNOWLEDGMENTS

The work was supported in part by a Grant in Aid, Ministry of Education, Science, Sport, Culture and Technology, Japan, the Japan Society for Promotion of Science, and the collaborative research grant from National Institute for Fusion Science, Japan (M.K.). A grant from the Institute for Theoretical Atomic and Molecular Physics at Harvard University and Smithsonian Astrophysical Observatory was also appreciated (M.K.). The Rice part of this project was supported by the Robert A. Welch Foundation under Grant C-1222, and by the National Science Foundation through Grant No. INT-9911858. R.J.B., J.P.G., and G.H. acknowledge financial support from the Deutsche Forschungsgemeinshaft grant Bu 450/7-3 and the Fonds der Chemischen Industrie. C.M.D. thanks Professor King Walters, Professor Pilip Brooks, and Dr. Bernard Lindsay of Rice University for useful discussions.

[1] A. Jorissen, V. V. Smith, and D. L. Lambert, Astron. Astrophys. **261**, 164 (1992).

[2] A. R. Ravishankara, A. A. Turnipseed, N. R. Jensen, S. Barone, M. Mills, C. J. Howard, and S. Solomon, Science **263**, 71 (1994).

[3] P. R. Larson, K. A. Copeland, G. Dharmasena, R. A. Lasell, M. Keil, and M. B. Johnson, J. Vac. Sci. Technol. B **18**, 307 (2000).

[4] *Agency for Toxic Substances and Disease Registry (ATSDR)* (U.S. Department of Health and Human Services, Public

Health Services, Atlanta, Georgia, USA, 2003).
[5] J. A. Tanis, A. L. Landers, D. J. Pole, A. S. Alnaser, S. Hossain, and T. Kirchner, Phys. Rev. Lett. **92**, 133201 (2004).
[6] M. Zamkov, E. P. Benis, C. D. Lin, T. G. Lee, T. Morishita, P. Richard, and T. J. M. Zouros, Phys. Rev. A **67**, 050703(R) (2003).
[7] A. G. Borisov, V. Sidis, P. Roncin, A. Momeni, H. Khemliche, A. Mertens, and H. Winter, Phys. Rev. B **67**, 115403 (2003).
[8] P. Roncin, A. G. Borisov, H. Khemliche, A. Momeni, A. Mertens, and H. Winter, Phys. Rev. Lett. **89**, 043201 (2002).
[9] J. P. Gu, G. Hirsch, R. J. Buenker, M. Kimura, C. M. Dutta, and P. Nordlander, Phys. Rev. A **62**, 052720 (2000).
[10] A. M. Arthurs, Proc. Cambridge Philos. Soc. **57**, 904 (1961).
[11] B. L. Moiseiwitsch, Proc. Phys. Soc. London **87**, 885 (1966).
[12] R. McCarroll and A. Salin, C. R. Seances Acad. Sci., Ser. B **263B**, 329 (1966).
[13] R. McCarroll and A. Salin, Proc. Phys. Soc. London **90**, 63 (1967).
[14] R. McCarroll and A. Salin, Proc. R. Soc. London, Ser. A **300**, 202 (1967).
[15] D. S. F. Crothers and A. R. Holt, Proc. Phys. Soc. London **81**, 75 (1966).
[16] M. Kimura, S. Chapman, and N. F. Lane, Phys. Rev. A **33**, 1619 (1986).
[17] M. Kimura, Phys. Rev. A **33**, 4440 (1986).
[18] M. Kimura, Phys. Rev. A **31**, 2158 (1985).
[19] D. Schneider, G. Nolte, U. Wille, and N. Stolterfoht, Phys. Rev. A **28**, 161 (1983).
[20] M. Kimura, S. Chapman, and N. F. Lane, Phys. Rev. A **33**, 1619 (1986).
[21] R. A. Phaneuf, M. Kimura, H. Sato, and R. E. Olson, Phys. Rev. A **31**, 2914 (1985).
[22] R. E. Olson and M. Kimura, Phys. Rev. A **32**, 3092 (1985).
[23] L. B. Zhao, P. C. Stancil, J.-P. Gu, H.-P. Liebermann, P. Funke, R. J. Buenker, and M. Kimura, Phys. Rev. A **71**, 062713 (2005).
[24] T. Kusakabe, L. Pichl, R. J. Buenker, M. Kimura, and H. Tawara, Phys. Rev. A **70**, 052710 (2004).
[25] M. Kimura and N. F. Lane, Phys. Rev. A **37**, 2900 (1988).
[26] M. Kimura, A. B. Sannigrahi, J. P. Gu, H. Hirsch, R. J. Buenker, and I. Shimakura, Astrophys. J. **473**, 1114 (1996).
[27] R. Suzuki, A. Watanabe, H. Sato, J. P. Gu, G. Hirsch, R. J. Buenker, and M. Kimura, Phys. Rev. A **63**, 042717 (2001).
[28] S. Suzuki, N. Shimakura, J. P. Gu, G. Hirsch, R. J. Buenker, M. Kimura, and P. C. Stancil, Phys. Rev. A **60**, 4504 (1999).
[29] L. Pichl, Y. Li, H.-P. Liebermann, R. J. Buenker, and M. Kimura, J. Chem. Phys. **118**, 4872 (2003).
[30] W. Fritsch, M. Kimura, and N. F. Lane, Phys. Rev. A **41**, 508 (1990).
[31] T. G. Winter, Phys. Rev. A **35**, 3799 (1987).
[32] T. G. Winter, Phys. Rev. A **25**, 697 (1982).
[33] T. G. Winter, Phys. Rev. A **43**, 4727 (1991).
[34] E. J. Shipsey, J. C. Browne, and R. E. Olson, J. Phys. B **14**, 869 (1981).
[35] D. R. Schultz, C. O. Reinhold, R. E. Olson, and D. G. Seely, Phys. Rev. A **46**, 275 (1992).
[36] R. J. Buenker and S. D. Peyerimhoff, Theor. Chim. Acta **35**, 33 (1974).
[37] R. J. Buenker and S. D. Peyerimhoff, Theor. Chim. Acta **39**, 217 (1975).
[38] R. J. Buenker, Int. J. Quantum Chem. **29**, 435 (1986).
[39] S. Krebs and R. J. Buenker, J. Chem. Phys. **103**, 5613 (1995).
[40] R. J. Buenker, in *Proceedings of the Workshop on Quantum Chemistry and Molecular Physics*, edited by P. G. Burton (University of Wollongong Press, Wollongong, Australia, 1980).
[41] R. J. Buenker and R. A. Phillips, J. Mol. Struct.: THEOCHEM **123**, 291 (1985).
[42] C. E. Moore, *Atomic Energy Levels*, NBS Circ. No. 467 (U.S. GPO, Washington, DC, 1971).
[43] M. Kimura and N. F. Lane, Adv. Astronaut. Sci. **26**, 79 (1989).